Oscillating Energy Harvester for UUV Applications

by

Lucas Kistner Stone

B.S., University of Pittsburgh (2010)

Submitted to the Department of Mechanical Engineering
in partial fulfillment of the requirements for the degrees of

Naval Engineer

and

Master of Science in Mechanical Engineering

at the

MASSACHUSETTS INSTITUTE OF TECHNOLOGY

June 2023

Author .....
Department of Mechanical Engineering
April 11, 2023

Certified by .....
Paul D. Sclavounos
Professor of Mechanical Engineering and Naval Architecture
Thesis Supervisor

Accepted by .....
Nicolas Hadjiconstantinou
Chairman, Department Committee on Graduate Theses

Oscillating Energy Harvester for UUV Applications

by

Lucas Kistner Stone

Submitted to the Department of Mechanical Engineering
on April 11, 2023, in partial fulfillment of the
requirements for the degrees of
Naval Engineer
and
Master of Science in Mechanical Engineering

Abstract

This thesis presents the design, modeling, and optimization of a novel oscillating energy harvester for use in a Bluefin-21 UUV. Real-world vessel acceleration data was used to optimize the harvester for four different potential energy profile configurations: free-floating, linear monostable, nonlinear monostable, and bistable. Active control was desired and two strategies were explored but deemed to be too costly to implement. The performance of each configuration was evaluated and it was found that the linear monostable model performed the best, although, due to detuning concerns, the free-floating configuration is expected to out perform the linear model across a range of sea state spectra. While the calculated power collection rate was insufficient for supplementing or recharging the main batteries, the harvester was found to be a promising alternative power source for an emergency location beacon, enabling continuous transmission as long as the UUV remained adrift. The findings of this thesis demonstrate the potential of oscillating energy harvesters in UUV applications and suggest avenues for further research into control strategies and experimental validation.

Keywords: oscillating energy harvester, UUV, floating, linear, nonlinear, monostable, bistable, control strategy

Thesis Supervisor: Paul D. Sclavounos
Title: Professor of Mechanical Engineering and Naval Architecture

Acknowledgments

I have many people to thank and acknowledge for their part in the completion of this research as well as the completion of my three year studies in the Naval Construction and Engineering Program.

First and foremost I would like to thank my thesis advisor, Professor Paul Sclavounos. To Professor Sclavounos, thank you for your continued guidance and support throughout this project. Your guidance and direction has been essential to the completion of this research and you have taught me so much through our weekly thesis meetings.

I would also like to thank the other student working in my lab, Alex Wunderlich. Although we worked on different applications of oscillating generators, I learned a great deal from you and greatly enjoyed our collaboration on the overall project.

To my 2N class of 2023, thank you for everything. From making the initial days of virtual classes seem less lonely and isolated to sharing your knowledge and collaborating on PSETs and group projects throughout our time here. I cannot imagine completing this program without your support and I cannot wait to see the success you all find in the years to come.

Last but not least, I would like to thank my family. To my parents and sister, thank you for your encouragement, always, but especially these last three years. To my beautiful wife, Casey, thank you for your continuous love and support. You kept me sane during stressful moments, understood when exams or projects came at inconvenient times, and accommodated the last minute zoom calls without question. All while being the keystone of our growing family. To my daughter, Clara, you become more and more amazing and wonderful every day. Thank you for every giggle, hug, and kiss. I love you both so much.

THIS PAGE INTENTIONALLY LEFT BLANK

Contents

List of Figures

List of Tables

THIS PAGE INTENTIONALLY LEFT BLANK

Chapter 1

Introduction

This thesis investigates an oscillating energy harvester designed specifically for Underwater Vehicle (UV) applications. Autonomous Underwater Vehicles (AUVs) and Unmanned Underwater Vehicles (UUVs) are becoming increasingly popular for both military and civilian applications, including research, ocean mapping, pipeline installation/inspection, and search & rescue. Most UVs are powered by rechargeable batteries which drive either a propeller or thrusters via an electric motor. The range and mission time of the UV is limited by the battery capacity. Additional batteries are costly both monetarily and in weight/space design tradeoffs onboard.

If an oscillating proof-mass energy harvester can be designed to recover energy from the motion of the UV, it can potentially augment the battery and increase the range and duration between recharges. Even if the harvester cannot capture enough energy to effectively supplement the main battery, it could still be useful as an alternative power source to an emergency location transmitter or beacon in the event the main batteries run down and the UV is adrift on the surface. A harvester that can capture enough energy from UV motion due to surface waves to power such a transmitter would remove the beacon's reliance upon onboard battery power and enable it to transmit indefinitely until recovered.

Research and development into energy harvesting from oscillations and mechanical vibrations has been actively pursued in both the micro-electromechanical systems (MEMS) and piezoelectric community [1] and the wave energy converter (WEC) community [15] over the past two decades . Many energy harvesters consist of linear oscillators which are only effective at near-resonance frequencies [19]. In addition to their narrow bandwidth, linear oscillators are susceptible to easy detuning, inefficiency in broadband and non-stationary excitations, and the difficulty of matching low-frequency excitations to resonance frequencies [10]. Different control strategies have been developed to adapt linear harvesters to behave as in resonance over a broader band of frequencies [15]. This control does expand the frequency range of device, but it is still limited to a relatively small range. Due to the inherently low-frequency, broadband, and non-stationary nature of ocean waves and vehicle motion, linear oscillators are not well suited to UV applications.

Attempts to overcome the limitations of linear oscillators have led to increased interest and research into nonlinear monostable and bistable oscillators. The use of permanent magnets and/or electromagnets has been demonstrated to be an effective method to produce both monostable [14] and bistable [19] nonlinear oscillators. However, nonlinear harvesters do not always outperform their linear counterparts. One reason for this is that nonlinear oscillations do not have a single unique solution, but co-existing low-energy and high-energy orbits [10]. Two methods have been shown to improve the performance of a bistable oscillator. The first is via the addition of a small excitation to modulate the potential energies of the two stability points [19]. The second is via an adaptive bistable potential operating under control strategy logic [10]. Adjustable electromagnets were used in both cases to achieve the desired result.

For oscillating harvesters, the excitation force injecting energy into the system is inertial and equals the product of the oscillating mass, m, and the acceleration of the container, $\ddot{\xi}$. In compact devices designed for MEMS and piezoelectric applications

the mass and displacement are typically very small, the frequency of oscillation is very high, and the energy generated is only in the microwatts to tens of watts range[1]. In scaling up an oscillation harvester for potential UV applications the mass and displacement will both be orders of magnitude larger than in MEMS devices, but the oscillation frequency will be small, sometimes only a fraction of a Hz. This low frequency coupled with the transient and broadbanded nature of the energy contained in the motions of underwater vehicles as well as the variance in their operating profiles both near and far below the free surface make UV oscillating harvester applications a unique challenge. Due to the low number of oscillations and the desire to extract as much energy as possible out of each one, electromagnetic induction is the most appropriate means of mechanical to electrical energy transduction due to its high power density.

The experience gained from the research and development within the MEMS community coupled with the high efficiency of electromagnetic transduction underscore the merits of exploring this technology for the marine environment. In this thesis I design an original oscillating energy harvester for UUV applications. Four different potential energy profile configurations of the harvester where modeled for comparison: free floating, linear monostable, nonlinear monostable, and bistable. Active control was desired and explored, but found to be too costly for this application. The background, theory, design concept and process are described in chapter 2. Chapter 3 presents the results for each of the four configurations. Areas for future work are discussed in chapter 4 and chapter 5 is the conclusion.

THIS PAGE INTENTIONALLY LEFT BLANK

Chapter 2

Oscillating Energy Harvester

2.1 Design Concept

The harvester is an axisymmetric device composed of a slider and a stator. The slider, also known as the proof mass, is a stack of ring magnets of alternating polarity with steel ring spacers in between each magnet. A fixed bar passes through the center of the stack and restricts the slider's motion to a single degree of freedom. The slider is affixed to the bar with low friction ball bearing bushings which allow smooth motion along the bar's axis. As the slider travels along the bar, it passes through the stator which includes three-phase coil windings. The basic arrangement of the slider and the stator is shown in figure 2-1. The length of the slider will be twice that of the

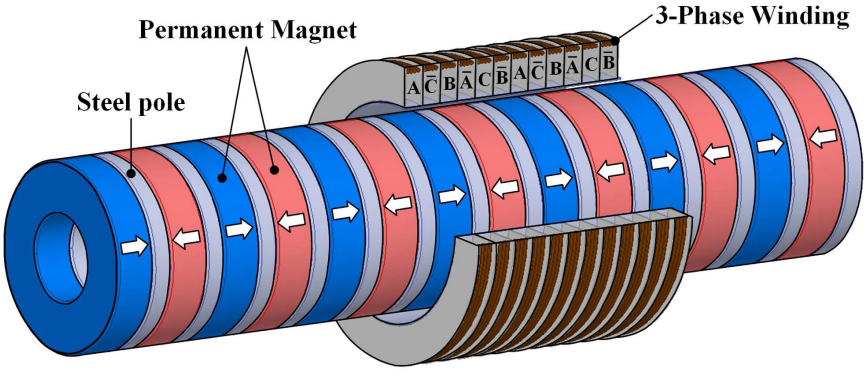

Figure 2-1: Representation of harvester slider and stator [12]

stator, and two thirds of the length of the bar from end-stop to end-stop. This limits the travel distance of the slider to be the same as the length of the stator and keeps the slider and stator fully magnetically coupled at all times.

As the alternating magnets of the slider pass through the stator they create a changing magnetic field through the wire coils which induces an electromotive force (emf) in the coil in accordance with Faraday's Law (equation 2.2) which in turn causes current to flow through the coils. The magnetic flux, Φ_B, in the coil is a function of the magnetic field, B, and the area of the wire coil, A. The induced emf, ϵ, and the current, i, are proportional to the rate of change of the magnetic flux. R_L is the useful load resistance and R_C is the parasitic ohmic resistance in the coils. The self-inductance of the coils is ignored at low frequencies. In our case, the change in magnetic flux is proportional to the velocity of the slider relative to the stator coils.

$$\Phi_B = \int B \cdot dA \tag{2.1}$$

$$\epsilon = i(R_L + R_C) = -\frac{\Delta \Phi_B}{\Delta t} = -\frac{\Delta \Phi_B}{\Delta x}\frac{\Delta x}{\Delta t} = -\gamma \dot{x} \tag{2.2}$$

$$i = \frac{-\gamma}{(R_L + R_C)}\dot{x} \tag{2.3}$$

The three-phase current generated in the stator coils will then be passed through a full-wave three-phase rectifier to supply a direct current, I_{DC}, to the battery or load. The output voltage, and current, of the full-wave three-phase rectifier are found via equation 2.4 where V_{RMS} is the root mean square of the three-phase voltage. Finally, the power delivered to the load is given by equation 2.5.

$$V_{DC} = \frac{3\sqrt{2}}{\pi} V_{RMS} \approx 1.35 V_{RMS} \tag{2.4}$$

$$P_L = I_{DC}^2 R_L = \frac{1.35^2 \gamma^2}{(R_L + R_C)^2}\dot{x}^2 R_L \tag{2.5}$$

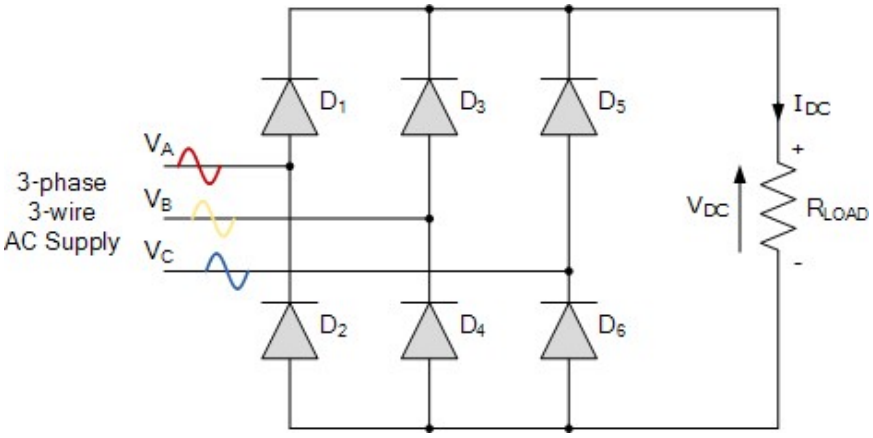

Figure 2-2: Full-wave Three-phase Rectifier [21]

From equation 2.5 it can be seen that the power to the load is proportional to the load resistance, over the square of the sum of the two resistances.

$$P_L \propto \frac{R_L}{(R_L + R_C)^2} \tag{2.6}$$

From this relationship is can be seen that for optimal power to the load the load resistance should be set equal to the resistance in the wire coils. The is referred to as impedance matching. For the rest of this thesis it is assumed that impedance matching is achievable via power electronics and $R_L = R_C$.

At each end of the bar will be a rubber bumper end-stop to constrain the maximum displacement of the slider. In conjunction with the bumper, different combinations of springs and/or end magnets will be used to explore monostable and bistable harvester designs, both linear and non-linear. A system without springs or end magnets would leave the slider free to float along the bar with no stable position. Springs, without end magnets, create a linear monostable system in which the proof mass will always return to the center of the bar. End magnets which repel the proof mass create a nonlinear monostable system. End magnets which attract the proof mass to each end create a bistable system with two potential energy wells, or stability points, where the proof mass will be held in place against an end-stop by the end magnet until an

external excitation force unseats and accelerates it toward to other end of the bar. In this final case the end magnets can be paired with springs to create the desired potential energy well and to quickly reduce the end magnet effects on the slider as it moves away from the end stop.

2.2 Equation of Motion

The harvester will be permanently mounted to the UUV frame with the slider being the only component which can move relative the the vessel. To accurately model the the motion of the slider along the bar, all forces acting upon it must be known and accounted for. Equation 2.7 is the equation of motion of the slider relative the frame and thus also relative to the stator.

$$m\ddot{x} = F_E(t) + F_{emf}(\dot{x}) + F_B(x) + F_S(x) + F_M(x) \tag{2.7}$$

- m is the mass of the slider, also know as the proof mass
- $x(t)$ is the displacement of the proof mass relative to the frame.
- $F_E(t)$ is the excitation force from the frame of the vessel
- $F_{emf}(\dot{x})$ is the damping force due to the induced emf in the coils
- $F_B(x)$ is the force from the rubber bumpers
- $F_S(x)$ is the force from springs
- $F_M(x)$ is the force from end magnets

2.2.1 Excitation Force

The only input into the system is the excitation force, $F_E(t)$, which has a magnitude equal to the mass of the slider times the acceleration of the frame.

$$F_E(t) = -m\ddot{\xi} \tag{2.8}$$

- $\ddot{\xi}$ is the acceleration of the vessel frame relative to Earth

2.2.2 Damping Force

The damping in the system has both a useful component which can be harvested and a parasitic component due to resistance loses in wire. Damping is proportional to the velocity of the slider relative to the stator.

$$F_{emf}(\dot{x}) = -\frac{1.35^2\gamma^2}{(R_L + R_C)}\dot{x} = -b\dot{x} \tag{2.9}$$

- b is the total damping coefficient, of which half is the useful damping from the load and the other half is the parasitic damping from ohmic losses in the coils

The power to the load, equation 2.5, can now be rewritten using the damping coefficient and simplified using the impedance matching assumption.

$$P_L = \frac{R_L}{(R_L + R_C)}b\dot{x}^2 = \frac{b}{2}\dot{x}^2 \tag{2.10}$$

2.2.3 Bumper Force

The bumper force, $F_B(x)$, is only present at the very ends of slider displacement and is zero everywhere else. The piece wise function, 2.11, was used for the bumper force

where the bumper itself was modeled as a very short and stiff spring.

$$F_B(x) = \begin{cases} -k_B x + (sign\{x\})k_B X_B & |x| \geq X_B \\ 0 & |x| < X_B \end{cases} \tag{2.11}$$

- k_B is the stiffness coefficient of the bumper
- X_B is the displacement where the slider will come into contact with the bumper

2.2.4 Spring Force

If the spring is always in contact with the slider, then the spring force is a linear function of displacement.

$$F_S(x) = -k_S x \tag{2.12}$$

- k_S is the stiffness coefficient of the spring

But if the slider only contacts a spring during part of the displacement path, then the spring force becomes a piece wise function similar to F_B.

$$F_S(x) = \begin{cases} -k_S x + (sign\{x\})k_S X_S & |x| \geq X_S \\ 0 & |x| < X_S \end{cases} \tag{2.13}$$

- X_S is the displacement where the slider comes into contact with the spring

2.2.5 End Magnet Force

The force from the end magnets is highest when the slider is at either end and decays rapidly as the slider moves away. Also, this force is adjustable by adjusting the spacing between the end magnets and the end stops. It was found that the end magnet force can accurately be modeled as a two term exponential function and scaled by the

maximum end magnet force, F_{Mmax}, which is a function of the spacing.

$$F_M(x) = |F_{Mmax}|(a\mathrm{e}^{cx} - a\mathrm{e}^{-cx}) \tag{2.14}$$

The process used to determine the end magnet force is described in detail in section 2.5.2.

The equation of motion, equation 2.7, neglects the effects of friction from air and in the ball bearings. Since air is free to flow around the outside of the coils from one side to the other, there is no air-damper effect in this design. There is couette air flow in-between the slider and the stator, but this effect was found to be negligible. High quality ball bearing are very efficient and friction between the bar and the bearings was also assumed to be negligible.

2.3 Control

Theoretically, the maximum efficiency of the harvester system would require an additional input for control. This control force, $F_C(x,t)$, could be from an electromagnet, a permanent magnet, or even a mechanical latch and would be used to control when the proof mass leaves an end stop. For example, let the maximum displacement of the proof mass, $x(t)$, be designated as distance Z from the center point of the bar, also stated as $|x(t)| \leq Z$. The excitation force, $F_E(t)$ is not affected by displacement, $x(t)$, and is known and measurable in real time from accelerometers mounted to the vessel frame. From the work of Halvorsen et.al. [8] in MEMS, it is optimal to hold the proof mass at an end stop until the excitation energy reaches it maximum value which will sling the proof mass to the other end. Explicitly, the proof mass should be held at $x = +Z$ while the derivative of the excitation force is less than zero, $\dot{F}_E(t) < 0$, and at the $x = -Z$ end stop while $\dot{F}_E(t) > 0$. When $\dot{F}_E(t) = 0$, the proof mass is released, allowing the excitation force to rapidly accelerate the proof mass toward the

other side. This strategy would require a control force capable of rapid adjustment and strong enough to prevent the excitation force from prematurely unseating the proof mass.

Two options for a control force were considered for this harvester design: electromagnets and rotating end magnets. Electromagnets are simple, cheap, easily customised, and favored in MEMS devices. Unfortunately, the control forces required are orders of magnitude higher than in MEMS applications and the frequency orders of magnitude lower. The higher forces require equivalently higher input energy and the lower frequency requires that energy input to be applied for longer time intervals. These combined affects raised the energy cost of electromagnets to an unacceptable level and removed them from consideration for this harvester.

A second option involving rotating the end magnets was deemed to require less input energy than an electromagnet and was explored further. Using the method proposed by Furlani [6] the torque required to rotate the end magnets and the changing control force during rotation were calculated. By substituting this control force for $F_E(x)$ in the equation of motion, the energy harvested with control was found and compared against the addition input energy required to overcome the torque and rotate the end magnets. While the harvester did collect up to three times more energy with control, the additional energy captured is less than the required input energy resulting in a lower overall energy balance. In light of this result, active control strategies were abandoned for this harvester, though additional research into active control strategies is encouraged for future research.

2.4 Representative UUV

In order to appropriately size the harvester and accurately model the motion of the vessel, a reference vehicle was needed. The bluefin-21 was selected as the representa-

tive medium sized UUV. This vessel was chosen because the navigation log data from a bluefin-21 research vehicle was made available to the lab. This data was collected by a navigation grade FOG INS unit (iXblue PHINS C7) and includes position, velocity, and acceleration of the UUV in surge, sway and heave every 0.1 second during a 2.5 hour mission in the Atlantic Ocean off the New England coastline. This real world data was used as an input into the equation of motion of the harvester to predict the amount of energy which could have been captured during this mission. Figure

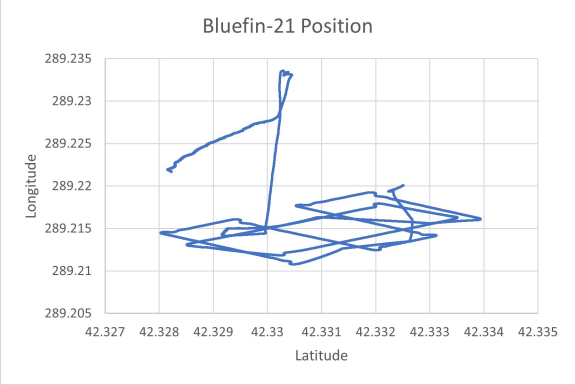

Figure 2-3: Latitude and longitude from bluefin-21 mission log

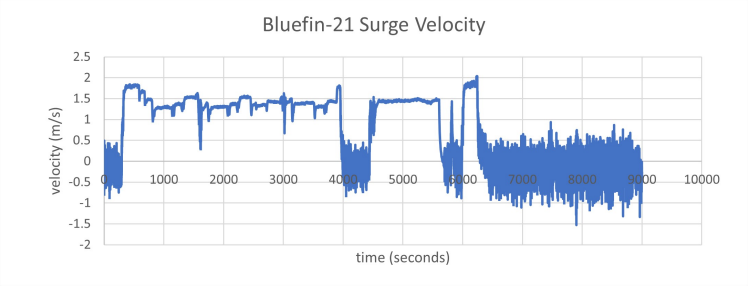

Figure 2-4: Surge velocity from bluefin-21 mission log

2-3 shows the path covered by the UUV in Latitude and Longitude. The UUV was operating submerged and under power for approximately half of this mission and drifting on the surface for the other half. These periods can be differentiated by the surge velocity, shown in figure 2-4, where a velocity greater than 1 meter per second indicates operational time. While operating submerged, the UUV is beneath the

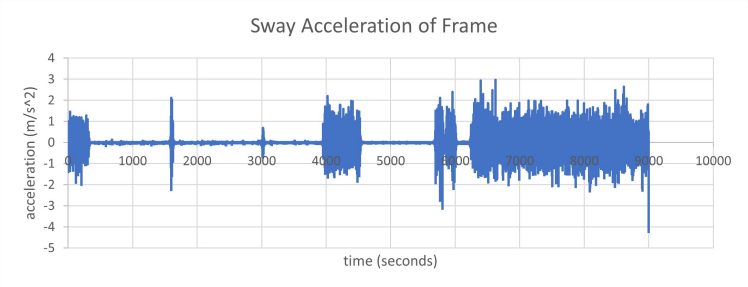

Figure 2-5: Sway acceleration from bluefin-21 mission log

wave action and any acceleration of the vehicle is predominately due to forces from the vehicles own propeller, thrusters, and control surfaces. When on the surface, the majority of forces and acceleration experienced by the UUV come from ocean waves. The force and energy input into the harvester is proportional to the sway acceleration of the UUV, figure 2-5. The sway acceleration is significantly higher during periods of surfaced drifting. By analyzing harvester performance during both submerged operations and surface drifting conditions the total energy capture potential for each period and the overall mission can be estimated and compared to the vessel's battery capacity of 13.5 kWh.

2.5 Slider and Stator Design

A three inch diameter neodymium ring magnet was chosen as the starting point for this design. This magnet is commercially available at K&J Magnets and its specifications are shown in figure 2-6. A model of the harvester was built in Solidworks (see figures 2-7 and 2-8) and in FEMM (Finite Element Methods Magnets, see figure 2-9). The slider is composed of 33 ring magnets (0.25" thick) and 32 iron spacers (0.125" thick) and has a length of 12.25".The slide bar has an overall length of 20.5" which just fits inside the diameter of the bluefin-21 at 53cm (20.87"). The stator is 6" long and includes an iron shell backing and the 3-phase coils which are split into 24 sections, eight for each phase. Assuming a fill facter of 0.8, each section can hold up

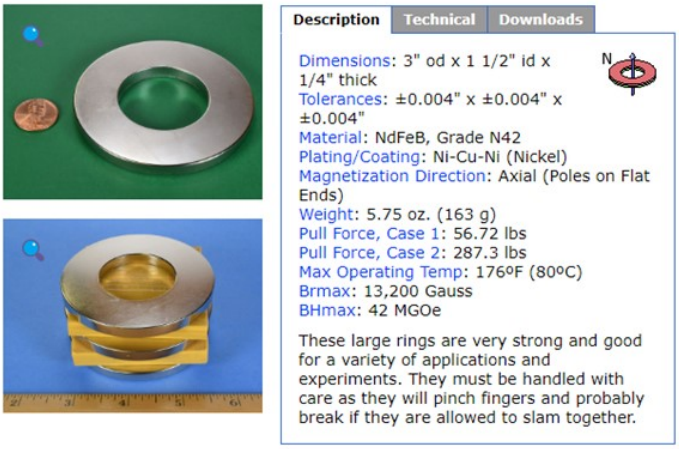

Figure 2-6: Ring magnet spec sheet from kjmagnetics.com

to 155 coils of 24AWG copper wire giving each phase a maximum total of 1240 coils. The exact number of coils is an adjustable parameter to allow for optimization of the system damping. The rubber bumpers of the end stops are 18.25" apart, allowing the slider 6" of travel. Figure 2-7 shows a labeled cut away view of the harvester with

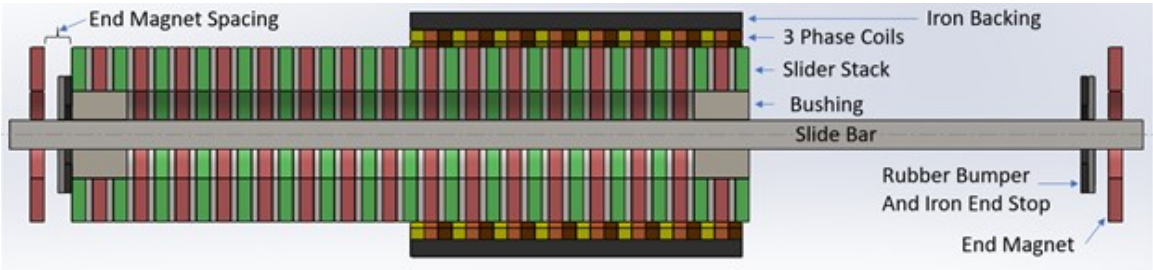

Figure 2-7: Cut away view of harvester with component labels

end magnets but no springs, and figure 2-8 is a scale drawing. The end magnets are the same 3" ring magnets used to make the slider and they are oriented to attract the slider to create a bistable system. The exact distance between the end magnet and the rubber bumper can be adjusted to control the strength of the potential energy well. As shown, the spacing between the end magnet and where the slider rests on the bumper is 0.5". (Design note: It was easier to build the model using English units since the base parts are sized in inches, but the analysis results from FEMM and Matlab are all in metric units.)

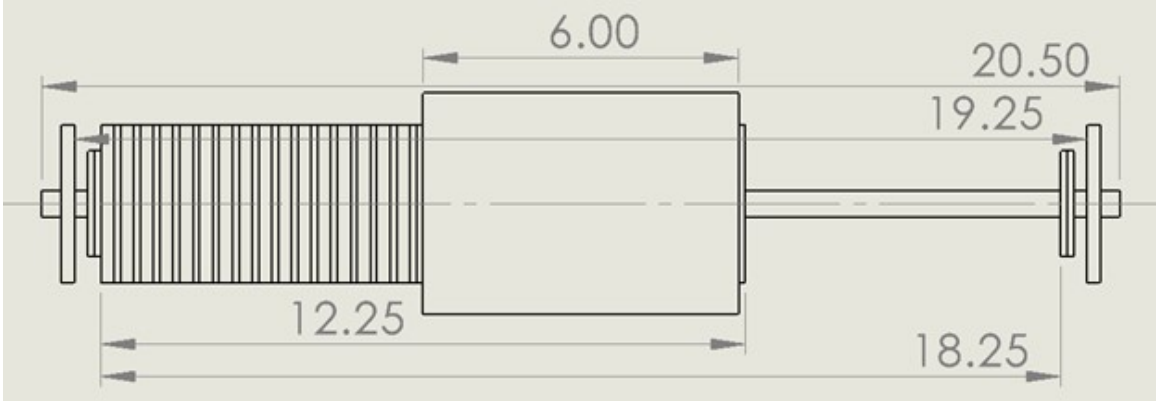

Figure 2-8: Scale drawing of harvester model (inches)

FEMM allows for axisymetric analysis, where only half of a cross section is built and the software then rotates it around the central axis prior to analysis. A half cross section of the FEMM model is paired with a half cross section of the Solidworks model in figure 2-9 to aid in visualizing the FEMM output. By modeling the three

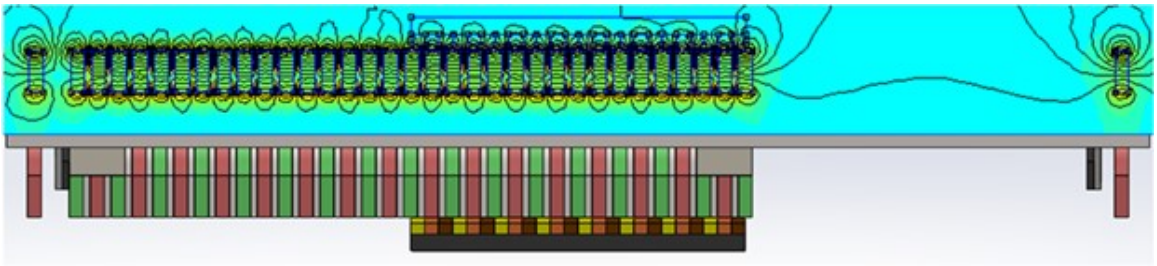

Figure 2-9: Havester modeled in FEMM

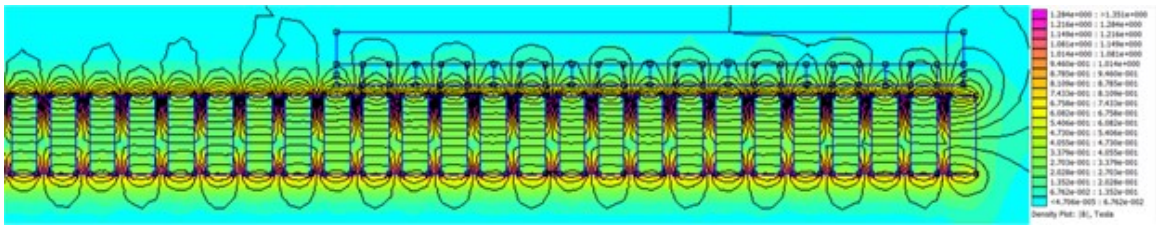

Figure 2-10: Magnetic flux, B, through wire coils

phases of windings as three separate circuits in FEMM, the total magntic flux linkage between the slider and each phase of windings is known. Using a lua script within FEMM, the slider position is varied in incremental steps from the left bumper to the

right bumper to obtain the total magnetic flux in each circuit as a function of slider position. From this data, the change in flux per change in slider displacement relative to the stator, know as the coupling coefficient γ, is easily calculated.

$$\gamma = \frac{\Delta \Phi_B}{\Delta x} \tag{2.15}$$

2.5.1 Proof Mass Weight Estimate

Using the densities of neodymium magnets and iron, the combined weight of the slider stack magnets and spacers was estimated to be $8.3kg$. The overall proof mass will also include the weight of the bushings and the sleeve and bracket assembly required to hold the slider stack together. The weight of these components is unknown as their design was beyond the scope of this thesis. To move forward, these additional weights were assumed to add up to $1.7kg$, giving the proof mass an estimated weight of $10kg$.

2.5.2 End Magnet Force

The force from the end magnets is highest when the slider is at either end and decays rapidly as the slider moves away. Also, this force is adjustable by adjusting the spacing between the end magnets and the end stops. A lua script was used in FEMM to find the magnetic force as a function of slider position at the minimum, middle, and maximum spacing. It was found that the shape of the force was the same across the adjustable range of the end magnets, and that a single normalized best fit function could be scaled by the maximum end magnet force to accurately model F_M for all spacing options. The curve fitter function in Matlab was used to fit a two term exponential function to the data.

$$F_M(x) = |F_{Mmax}|(a\mathrm{e}^{cx} - a\mathrm{e}^{-cx}) \tag{2.16}$$

$$a = 0.0008648 \quad c = 92.56$$

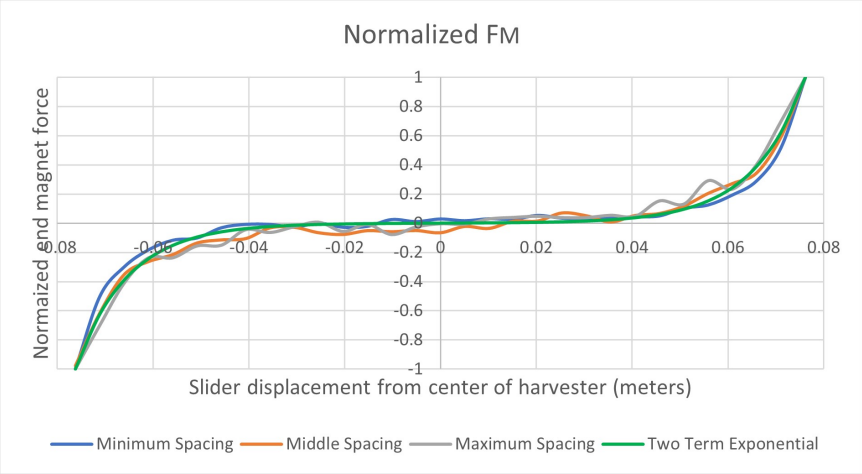

Figure 2-11: Normalized End Magnet Force

S *cm (in)*	F_{Mmax} N
0.635 (0.250)	152.7
0.953 (0.375)	96.6
1.270 (0.500)	63.5
1.588 (0.625)	42.8
1.905 (0.750)	28.8

Table 2.1: F_{Mmax} values over Spacing range

Figure 2-11 shows the normalized end magnet force as a function of proof mass displacement for the minimum, middle, and maximum spacing options as well as the best fit two term exponential function used to model F_M moving forward. Table 2.1 shows the maximum end magnet force, F_{Mmax}, for five different spacing options including the minimum, middle, and maximum. Spacing, S, is defined as the gap between the end magnet and the slider stack when the slider is at its maximum displacement.

If an $F_{Mmax} < 28.8N$ is desired, the selected end magnet can be replaced with a less powerful magnet or even an iron ring. The stack magnets of the slider will still react with the lesser magnet or iron, but the force will be reduced. Using this technique the F_{Mmax} can be varied all the way down to near zero. The end magnet

force profile in figure 2-11 is for when the end magnets are attracting the slider toward the ends. To find the profile for end magnets which are repelling the slider, simply multiply equation 2.14 by (-1).

2.6 Energy Capture Calculation

A matlab script was built to solve the previously described equation of motion. Specifically, the ODE45 solver was used to solve the system of differential equations dependant on both displacement and time, $\ddot{x} = f(x, t)$. User inputs are used to include or remove springs and/or end magnets. Additionally, the spacing and polarity of end magnets, the stiffness and length of springs, and the back emf damping (i.e. the number of coils per phase) are adjustable. With these levers, the type of harvester (i.e. floating, monostable, bistable, linear, nonlinear, etc) can be selected and performance of the harvester optimized for the selected type.

2.6.1 Excitation Force

To use the raw sway acceleration data from figure 2-5 as an input to the ODE45 solver, it must first be represented as a continuous function of time. This was accomplished using a Fourier series approximation script [20] available on the MathWorks file exchange. A representative two minute segment of acceleration data was fed into the script to obtain a high order (150 term) Fourier series fit function. A graphical representation of the raw acceleration data and the corresponding Fourier series function for submerged operations and surfaced drifting can be seen in figures 2-12 and 2-13 respectively. The corresponding excitation force is found from equation 2.8. The fourier series fit function for surfaced drifting, figure 2-13, is an excellent match to the raw data, but the fit function for submerged operations, figure 2-12, shows more deviation from the data points. This is believed to be due to the very

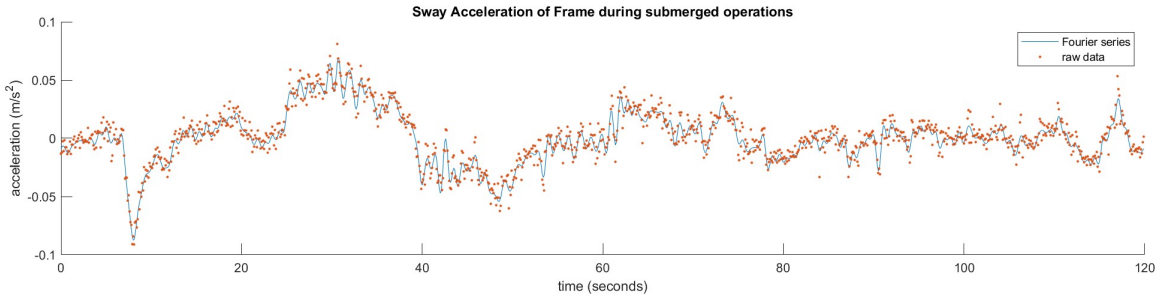

Figure 2-12: Fourier series fit function for sway acceleration during submerged operations

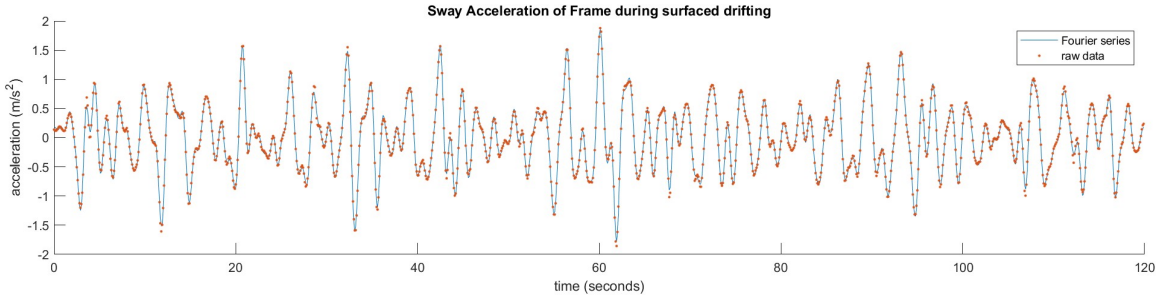

Figure 2-13: Fourier series fit function for sway acceleration during surfaced drifting

small accelerations experienced while submerged, and the sensitivity of the sensors collecting the data. The fit function for submerged operations did not appreciable improve with more terms, so it was left at 150 terms.

It should be noted that the acceleration experienced while operating submerged is more than a order of magnitude less than the accelerations while drifting on the surface. The excitation forces will be similarly disparate. This is an early indication that their is significantly more harvest-able energy on or near the surface, and that the harvester should be optimized for surfaced drifting conditions.

2.7 Maximum Theoretical Power

Using the excitation force from the acceleration fourier series fit functions described above, the maximum theoretical power was calculated for both submerged operations

and surfaced drifting conditions using equation 2.17.

$$P_{TH} = \frac{b}{2}\sum_{j=1}^{150} C_j^2 \frac{m^2\omega_j^2|H_{\ddot{\xi}}(\omega_j)|^2}{m^2\omega_j^4 + b^2\omega_j^2} = \frac{b}{2}\sum_{j=1}^{150} C_j^2 \frac{|H_{\ddot{\xi}}(\omega_j)|^2}{\omega_j^2 + (\frac{b}{m})^2} \tag{2.17}$$

- $j = 1...150$ counts each term in the 150 term fourier series used to represent the real world acceleration data from the bluefin-21 mission
- C_j is the combined amplitude of the fourier series amplitudes, A_j and B_J. Where $C_J^2 = A_j^2 + B_j^2$
- ω_j is the frequency steps maped in the fourier series
- $H_{\ddot{\xi}}(\omega_j)$ comes from the fourier transform of the acceleration of the vessel frame relative to Earth

$$\ddot{\xi}(t) = Re\{\sum_{j=1}^{150} C_j H_{\ddot{\xi}}(\omega_j) e^{i\omega_j t + i\phi_j}\} \tag{2.18}$$

From equation 2.17, the theoretical power is proportional to the damping term, b, in the numerator, but it is also affected by the $(\frac{b}{m})^2$ term in the denominator. To maximize the power, it is desirable to maximize b while minimizing $\frac{b}{m}$. If the mass, m, was an adjustable variable, then increasing the mass is an easy solution. In this device, the mass is assumed to be fixed at $10kg$. The damping, b was varied from zero up to $74\frac{Ns}{m}$, which is the maximum achievable based on the maximum number of coils which can fit into the stator. The optimal damping was found to be $b = 2\frac{Ns}{m}$ during submerged operations and $b = 22\frac{Ns}{m}$ when the UUV was drifting on the surface. The respective power profiles can be seen in figure 2-14 and figure 2-15. By integrating over the frequency range where the power is above zero, the maximum theoretical power was found to be $P_{TH} = 0.006watts$ during submerged operations and $P_{TH} = 0.334watts$ while drifting. The achievable power while drifting on the surface is two orders of magnitude greater than when operating submerged. This confirms the earlier assumption that there is little to no harvest-able energy away

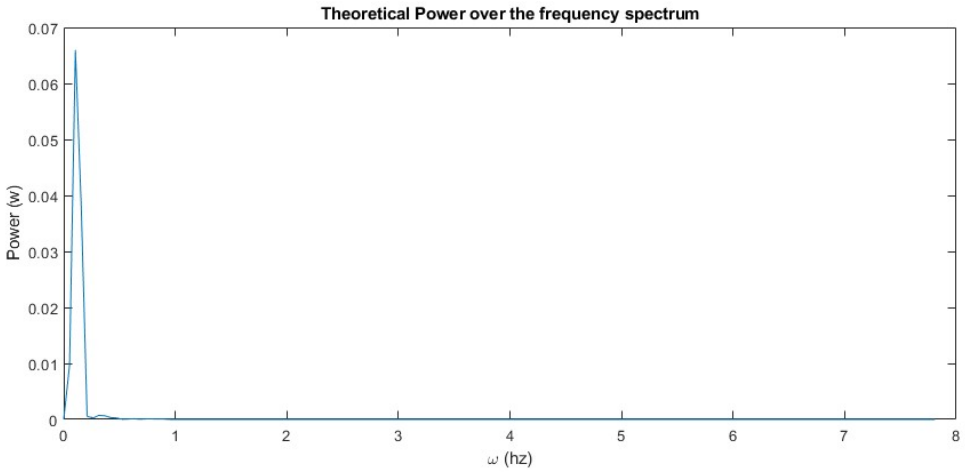

Figure 2-14: Power profile @ b=2 Ns/m, submerged operating

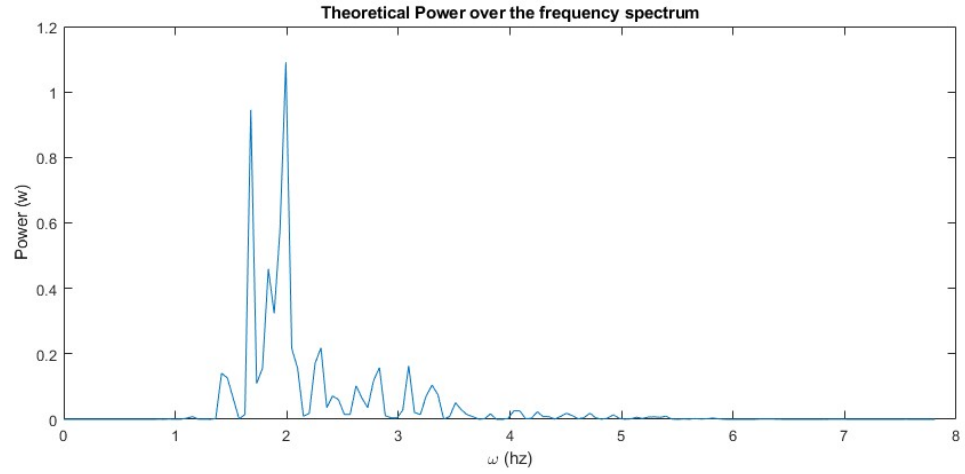

Figure 2-15: Power profile @ b=22 Ns/m, surfaced drifting

from the ocean surface. The harvester design shall be optimized for the surfaced drifting condition.

Chapter 3

Harvester Configurations

In this thesis, four different potential energy profile configurations for the oscillating energy harvester were considered. Each of these configurations were then optimized for energy collection under surfaced drifting conditions.

3.1 Configuration 1: Free Floating

The free floating harvester is the simplest design and considered the baseline. This configuration has neither springs nor end magnets, and the slider is unconstrained as it travels between the bumpers. The equation of motion for this configuration can be simplified and re-written as equation 3.1 when the slider is not in contact with a bumper and as equation 3.2 when the slider is in contact with an end bumper.

$$m\ddot{x} + b\dot{x} = -m\ddot{\xi} \tag{3.1}$$

$$m\ddot{x} + b\dot{x} + k_B x - (sign\{x\})k_B X_B = -m\ddot{\xi} \tag{3.2}$$

The total damping coefficient, b, is the only adjustable parameter in this configuration. The maximum theoretical power equation, 2.17, was derived from equation 3.1 and it was assumed that the optimal damping coefficient found in section 2.7 would still

be the optimal setting for this configuration. But the theoretical model allows for infinite travel of the slider, i.e. it is not constrained by bumpers. If the bumpers are "removed" from the equation of motion, then the model behavior is in line with the predicted values and has the same optimal damping of $b = 22\frac{Ns}{m}$ and an average power of $P = 0.302watts$; 90% of the theoretical maximum. In reality, the displacement of the slider must be constrained and the bumpers cannot be removed. With the bumpers in place, the harvester is less efficient and the optimal damping is higher than in the unconstrained case. The optimal damping coefficient is now $b = 43\frac{Ns}{m}$ and the average power is $P = 0.227watts$; which is 90% of the theoretical power @ $b = 43\frac{Ns}{m}$ but only 68% of the maximum theoretical power @ $b = 22\frac{Ns}{m}$. The response of the energy harvester over a two minute period can be seen in figure 3-1. The free floating harvester is predicted to collect 27.2 joules every two minutes while drifting. At this rate, the harvester will collect 816 joules every hour.

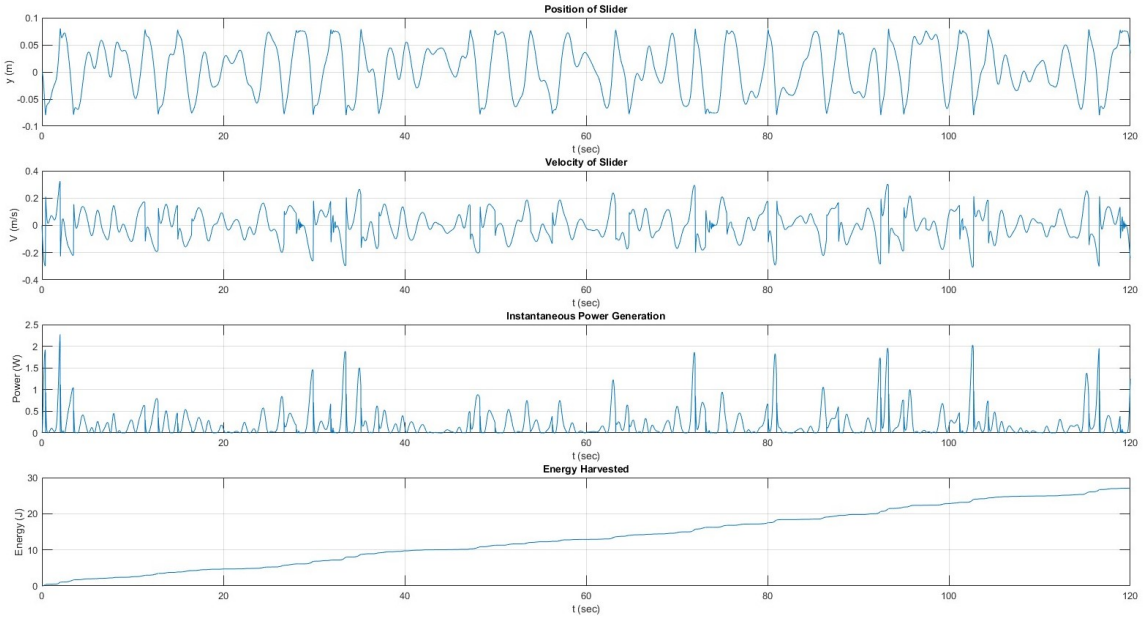

Figure 3-1: Free Floating Energy Harvester Results

3.2 Configuration 2: Linear Monostable

The linear monostable harvester can be modeled as the familiar spring-mass-damper system. The spring is in it's neutral position when the slider is centered between the two end bumpers. Thus, after a perturbation, the spring will always return the slider to the center point of the harvester. The equation of motion is simplified and re-written as equation 3.3 when the slider is not in contact with a bumper and as equation 3.4 when the slider is in contact with an end bumper.

$$m\ddot{x} + b\dot{x} + k_S x = -m\ddot{\xi} \tag{3.3}$$

$$m\ddot{x} + b\dot{x} + k_S x + k_B x - (sign\{x\})k_B X_B = -m\ddot{\xi} \tag{3.4}$$

The total damping coefficient, b, and the spring constant, k_S, are each adjustable parameters in this configuration. The natural frequency, ω_n, is a function of the spring constant.

$$\omega_n = \sqrt{\frac{k_S}{m}} \tag{3.5}$$

The optimal ω_n for the theoretical case without bumpers is $1.95Hz$, ($k_S = 38\frac{N}{m}$) as predicted in figure 2-15. When the bumpers are present, constraining the maximum displacement of the slider, the optimal natural frequency and spring constant both drop. The optimal settings for this configuration are $b = 43\frac{Ns}{m}$ and $k_S = 19\frac{N}{m}$ which result in an average power harvested of $P = 0.232watts$. The response of the energy harvester over a two minute period is shown in figure 3-2. The linear monostable harvester is predicted to collect 27.9 joules every two minutes while drifting. At this rate, the harvester will collect 836 joules every hour. This is only 20 joules more than the free floating configuration, an increase of just 2.5%.

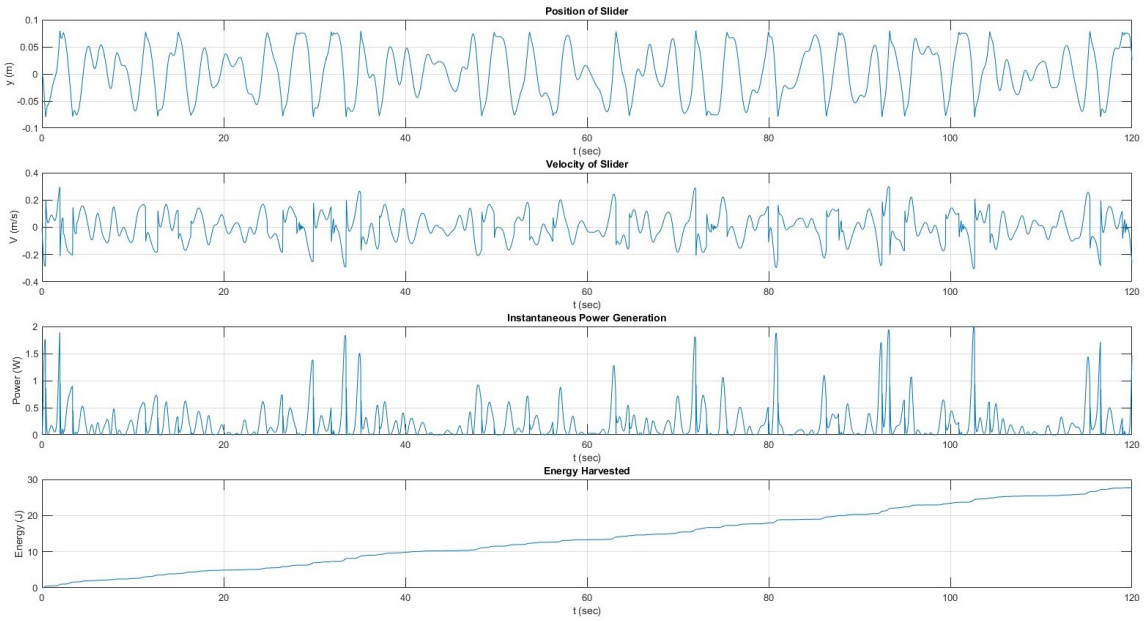

Figure 3-2: Linear Monostable Energy Harvester Results

3.3 Configuration 3: Non-Linear Monostable

In the non-linear monostable harvester the springs are replaced by end magnets which repel the slider stack away from each end. In this configuration the end stops and bumpers are not required, since the repulsive force between two magnets increases exponentially as the distance between them decreases. The end magnets will prevent the slider from ever physically exceeding its maximum allowed displacement. The equation of motion is simplified and re-written as equation 3.6.

$$m\ddot{x} + b\dot{x} + |F_{Mmax}|(a\mathrm{e}^{cx} - a\mathrm{e}^{-cx}) = -m\ddot{\xi} \tag{3.6}$$

The total damping coefficient, b, and the maximum end magnet force, F_{Mmax}, are each adjustable parameters in this configuration, though the end magnet force must be strong enough properly constrain the slider. The optimal settings for this configuration are $b = 49\frac{Ns}{m}$ and $F_{Mmax} = 37N$ which result in an average power harvested of $P = 0.200watts$. The response of the energy harvester over a two minute period

is shown in figure 3-2. The non-linear monostable harvester is predicted to collect 24.0 joules every two minutes while drifting. At this rate, the harvester will collect 720 joules every hour. This is 96 joules less than the free floating configuration, a decrease of 12%.

The optimization for this configuration wanted to reduce the strength of the end magnets to zero, which is equivalent to the free floating design without bumpers. But the maximum slider displacement must be constrained by the end magnets, which greatly reduced the efficiency. The power harvested was slightly improved by increasing the damping coefficient, but not enough to match the free floating design.

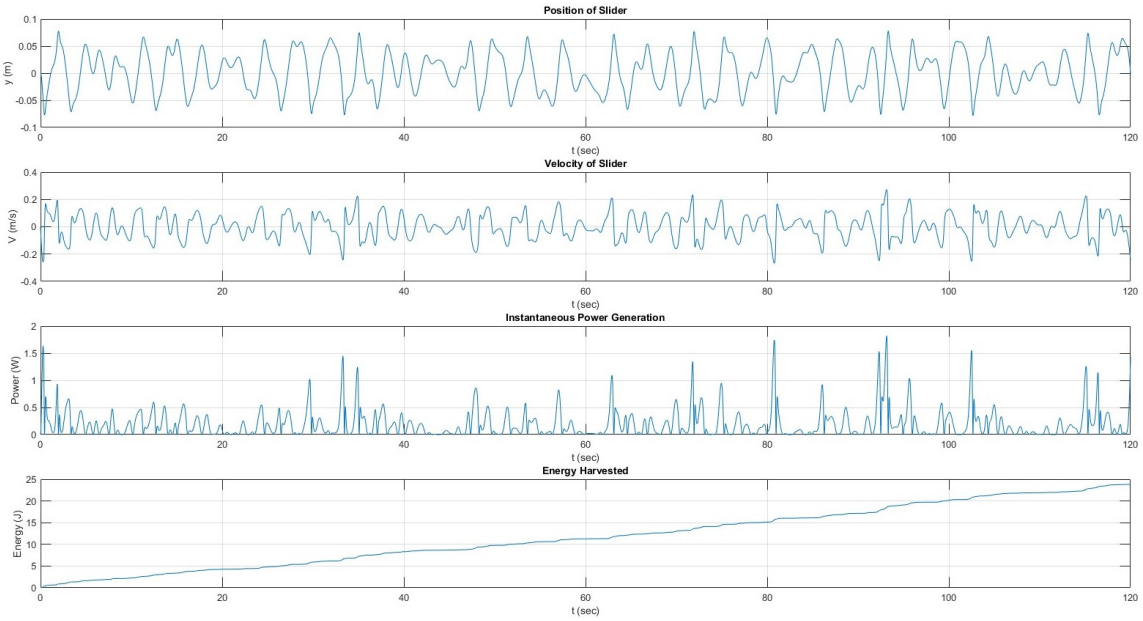

Figure 3-3: Non-Linear Monostable Energy Harvester Results

3.4 Configuration 4: Bistable

In the bistable harvester the end magnets are flipped, so that they now attract the slider stack. Springs are incorporated to counter the end magnet force and quickly reduce the effects of the magnets away from the ends. These springs are not in

continuous contact with the slider like the springs used in the linear harvester. Instead, these springs will only engage with the slider near the ends of the travel path. Bumpers are required to prevent the slider from exceeding its maximum displacement and slamming into the end magnets. Ideally, the end magnet would 'release' the proof mass when the external force reaches a local maximum. This would impart the greatest excitation force and acceleration upon the proof mass and result in the highest slider velocity relative to the stator. Unfortunately, due to the broadband and non-stationary nature of ocean waves, there is not a consistent 'maximum' value. Instead a full spectrum of the wave input excitation forces must be considered, and the force required to unlatch must be matched to the overall spectrum. If the unlatching force is too high, the slider will remain stationary at one end for the majority of the spectrum and only transition with the occasional high energy wave. In this case the harvester would collect more energy per trip, but with only a few trips total, the overall energy capture would be low. Conversely, if the release energy is too low then the proof mass will unseat earlier than desired, resulting in lower slider velocity and lower energy capture per trip.

The equation of motion for this configuration can be simplified and re-written as equation 3.7 when the slider is not in contact with a bumper or spring, as equation 3.8 when the slider is in contact with a spring only, and as equation 3.9 when the slider is in contact with a spring and bumper.

$$m\ddot{x} + b\dot{x} - |F_{Mmax}|(a\mathrm{e}^{cx} - a\mathrm{e}^{-cx}) = -m\ddot{\xi} \tag{3.7}$$

$$m\ddot{x} + b\dot{x} - |F_{Mmax}|(a\mathrm{e}^{cx} - a\mathrm{e}^{-cx}) + k_S x - (sign\{x\})k_S X_S = -m\ddot{\xi} \tag{3.8}$$

$$m\ddot{x}+b\dot{x}-|F_{Mmax}|(a\mathrm{e}^{cx}-a\mathrm{e}^{-cx})+(k_S+k_B)x-(sign\{x\})(k_S X_S+k_B X_B) = -m\ddot{\xi} \tag{3.9}$$

The total damping coefficient, b, the maximum end magnet force, F_{Mmax}, the spring constant, k_S, and the displacement where the slider first contacts the spring, X_S, are

all adjustable parameters in this configuration. The springs should be used to cancel out the end magnet force away from the ends and result in a near zero combined force across as much of the travel path as possible. The concept is illustrated in figure 3-4 where the combined force is near zero for displacements between $-6 < x < 6\ cm$.

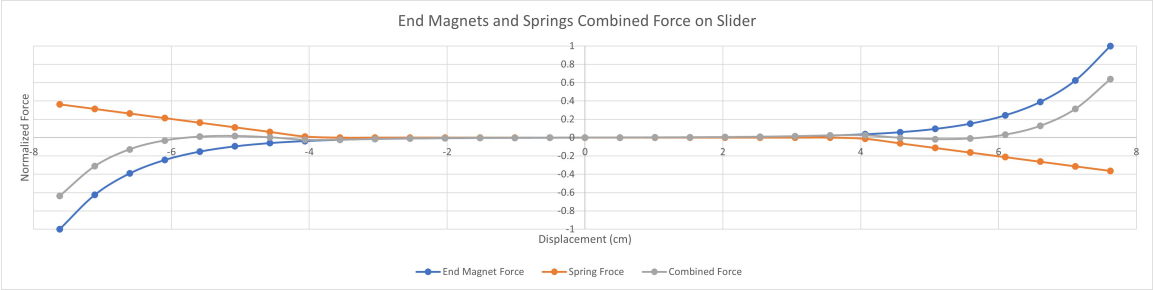

Figure 3-4: Combined End Magnet and Spring Force

The optimal settings for this configuration are $b = 41\frac{Ns}{m}$, $F_{Mmax} = 28.8N$, $k_S = 825\frac{N}{m}$, and $X_S = 4.7cm$ which result in an average power harvested of $P = 0.227watts$. The response of the energy harvester over a two minute period is shown in figure 3-5. The bistable harvester is predicted to collect 27.3 joules every two minutes while drifting. At this rate, the harvester will collect 819 joules every hour. This is just 3 joules more than the free floating configuration, an increase of only 0.4%.

The end magnet force, $F_{Mmax} = 28.8N$ is the minimum force obtainable when the end magnet is the same neodymium ring magnet used to build the slider stack. Forces below this value would be achievable using a less powerful end magnet, and this option was explored. A lower end magnet force, when appropriately matched with k_S and X_S, can match the power output achieved above, but no combination was found which exceeded the previous value of $P = 0.227watts$.

3.5 Results Summary

A summary of the results described above is provided in table 3.1. Of the four configurations, the linear monostable harvester preformed the best, collecting 2.5%

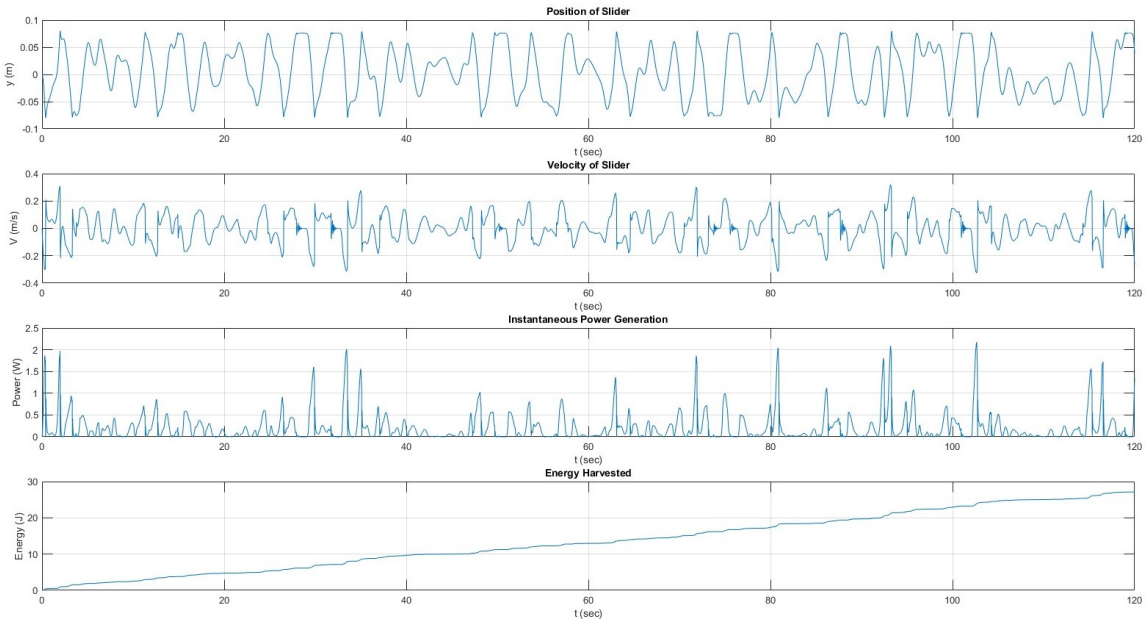

Figure 3-5: Bistable Energy Harvester Results

more energy than the free floating harvester. The free floating and the bistable configurations performed equally well and the non-linear monostable preformed the worst, collecting 12% less energy than the free floating harvester.

Configuration	Average Power W	Energy Harvested J/hr	b Ns/m	k_S N/m	X_S cm	F_{Mmax} N
Floating	0.227	816	43	N/A	N/A	N/A
Linear	0.232	836	43	19	0	N/A
Non-Linear	0.200	720	49	N/A	N/A	37
Bistable	0.227	819	41	825	4.7	28.8

Table 3.1: Summary of Results

While the linear harvest did preform the best in this study, it must be remembered that the excitation force from the acceleration of the vessel frame was only modeled over a two minute interval, and that the parameters for the linear harvester were optimized for this specific excitation force model. Even a slight deviation in the sea state spectrum could result in detuning the linear harvester and a significant drop in harvester efficiency. For this reason, the linear harvester is not anticipated to consistently out preform the free floating harvester under real world conditions. The

bistable harvester is capable of matching the output of the free floating harvester, but it is also more susceptible to detuning due to changes in the sea state. Additionally, it is a more complex design which would be more expensive to build and require more maintenance.

The free floating harvester is the simplest design and thus the cheapest to build and maintain. It is less susceptible to detuning than the more complex designs, and is thus expected to be more capable at harvesting energy over a range of sea state spectrums. For these reasons the free floating harvester design is recommended for UUV applications.

3.6 Cost/Benifit Analysis

The bluefin-21 has a battery capacity of $13.5kWh$ and an endurance estimate of 25 hours at 3 knots. From these values it is estimated that UUV requires $0.54kW$ of energy to maintain a speed of 3 knots. From the bluefin mission data, the UUV was operating under power for approximately half of the 2.5 hour mission. During those operational periods the average speed was 2.7 knots. Using linear interpolation and airing on the side on conservatism, it is estimated that the average energy usage for the bluefin during the operation periods of the mission was $0.5kW$ and the total energy consumption for the mission was $0.625kWh$ or $2250kJ$.

The UUV spent the other half of the mission drifting on the surface. If the free floating harvester had been installed on this UUV then it is estimated that it would have collected $1.02kJ$ or about $0.0003kWh$. This is less than 0.05% of the energy expended during the operational half of the mission. At this rate it would take 115 days of surfaced drifting for the harvester to replace the energy used during the 75 minutes of operational time during this mission.

The oscillating energy harvester is not going to be an efficient nor reasonable

means of recharging the main batteries of the UUV. However, it does collect enough energy to power an emergency locating beacon. Such beacons are usually powered by their own, separate batteries. The capacity of these batteries, and their operational battery life once activated, vary widely based on size and design. The beacon currently used on the bluefin-21 is not known, and thus direct comparison to the oscillating harvester is not possible. The advantages of a separate battery pack for the beacon include potential space and weight savings compared to the oscillating harvester. The advantage of the harvester would be a theoretically infinite "battery life" as long as the UUV was floating on the surface.

3.6.1 Dollar Cost Estimate

The most expensive component of the harvester will be the neodymium magnets. The shaft, bearings, spacers and bumpers are all easily attainable and cheap. Even the required power electronics hardware is common and inexpensive. The 3" diameter neodymium ring magnets used in this design are sold individually for $36.54, but can be bought in bulk for as low as $30 each. There are 33 ring magnets in the slider. Assuming they were bought at the discounted price, just the magnets for a single harvester would cost $990. Assuming the rest of the components could be obtained for a quarter of this price, the total cost for a single harvester is estimated to be around $1250.

Chapter 4

Future Work

There are multiple aspects of an oscillating energy harvester for UUVs which warrant further investigation.

4.1 Stator and Slider Design

The goal of this thesis was not to optimize the magnetic coupling of the stator and slider, but instead to explore the affects of different potential energy architectures. There are already multiple sources available on the topic of magnetic coupling optimization for linear generators. Possibilities for improvements include using a Halbach array with flux guide teeth to strengthen and shape the magnetic flux field over the coils, exploring thinner ring magnets and spacers to optimize the coupling coefficient, and backplate and spacer thickness optimization without exceeding the magnetic flux density saturation point.

While these potential improvements exist, they would not necessarily result in any improvement in energy harvested. The result of improving the magnetic coupling would be to increase the maximum achievable damping coefficient, b. The current design can achieve a damping coefficient of $74\frac{Ns}{m}$, which is far greater than the modeled optimum damping of $43\frac{Ns}{m}$. Only when the desired optimal damping is greater

than the maximum achievable damping should magnetic coupling improvements be pursued.

4.2 Mass and Maximum Displacement

As discussed in the maximum theoretical power discusssion in section 2.7, the power harvested is proportional to the damping term, b, in the numerator, but it is also affected by the $(\frac{b}{m})^2$ term in the denominator. To maximize the power, it is desirable to maximize b while minimizing $\frac{b}{m}$. If the mass, m, was an adjustable variable, then increasing the mass is an easy solution. In this thesis, the mass was essentially fixed by the choice of ring magnet used in slider assembly. If there is both space and ballast margin available inside a given UUV, then the dimensions of the slider stack should be chosen as to maximize the mass.

Similarly, section 3.1 revealed that constraining the maximum displacement of the slider reduced the power from $0.302 watts$ to $0.227 watts$, a decrease of 25%. While the slider displacement must always be constrained in real world applications, if the constraint is such that the slider never contacts the bumpers during normal operations then much, or all, of the theoretical maximum power could be achieved. In this thesis, the constraint was already set at the maximum value allowed by the diameter of the bluefin-21 UUV. A further balancing of mass and damping should be assessed to determine if a combination was possible for which the slider would not contact the bumpers during normal operations, and if so, how does the power compare to the current design's realized power. It is anticipated that to achieve this natural motion between the bumpers the mass of the slider would have to be reduced, which would reduce the power potential as discussed above, and erase any potential gains in efficiency. This belief comes from limited experimentation with the existing model; a more detailed analysis would be required to verify the results.

Instead of a single oscillating harvest it might be beneficial to incorporate a large number of smaller harvesters. The smaller mass of the individual sliders would facilitate achieving a greater efficiency; closer to the unconstrained device as described above. While each individual harvester would have a smaller mass, and thus capture less energy, the combined mass of multiple smaller harvester could match or exceed the mass of the single, bigger, harvester. This concept also introduces the option for an array of linear energy harvesters, each tuned to a different natural frequency. The broadened bandwidth of such a passive array, when properly matched to the ambient sea state spectrum could minimize the risk of detuning any single harvester and is worthy of further investigation.

4.3 Control

Multiple previous works in the MEMS community, including Halvorsen et.al. [8], Hooseinloo and Turitsyn [10], Su et.al. [19], and Mallick et.al. [13], have shown that control can be used to improve the net energy of oscillating harvesters. Two sources of a control force were investigated in this thesis, electromagnets and rotating end magnets. Neither option was deemed operationally feasible due to the high energy costs of implementation. Theoretically, an effective control strategy still offers efficiency gains, and further research in this area is encouraged. A specific type of control which is of interest is a mechanical latch mechanism that will hold the proof mass at the end until the optimum conditions for release have been met. The latch must be durable, quick to respond, and relatively "cheap" to activate.

An alternative form of control would be to design the parameters of the harvester, such as damping or the spring constant, to be adjustable. This form of control could be active, with a logic loop which adjusts the parameter continuously, or passive with the parameters set manually prior to each mission. This form of control would

reduce the risk of detuning in the linear and bistable harvester configurations and potentially enable these versions to equal or exceed the performance of the free floating configuration over a range of sea state spectra.

4.4 Harvester Construction and Testing

The oscillating harvester designed in this thesis should be built. This would allow for experimentation and testing to compare against the predicted model results. Additionally, the harvester can be subjected to a range of ocean environments and sea state spectra to determine the effects of detuning upon the different configurations and test the hypothesis that the free floating configuration will be the most efficient harvester over a range of spectra.

Finally, the alternative form of control via adjustable damping, spring constant, etc. as described above can be tested. If the improved efficiency of the linear harvester can be consistently achieved over a range of sea states via these adjustments, then it would become the preferred model for future applications.

4.5 Feasibility Study

Finally, a study should be preformed to determine if the oscillating harvester delivers enough energy to be worth the space and weight is occupies inside the UUV. Underwater vehicles are either space limited, weight limited, or both. This harvester would only occupy approximately 0.1% of the volume inside the bluefin-21, but it must be located across the center of the UUV which is the only place where the harvester will fit. This is prime real estate in underwater vessels, as all large and/or cumbersome equipment must fit in this location. Possibly even more concerning, the bluefin-21 only has $7.3kg$ of net positive buoyancy. This is the buoyancy which brings the UUV to the surface when not operating and is also a safety feature as it aids in vehicle

recovery in the event of component failure or a dead battery. The slider alone in this harvester weights $10kg$. Including the stator, slide bar with stops, and power electronics the overall harvester weight is estimated to be $15kg$. Meaning that if the harvester was added to the bluefin-21 as is, the UUV would have a $7.7kg$ net negative buoyancy. It would sink and be lost. It is possible that the bluefin has $15kg$ of ballast weight which could be removed in exchange for the harvester. If not, then the $15kg$ would potentially have to come out of the payload. These potential costs must be weighted against the desirability for an indefinite power supply for the emergency locating beacon.

A better application for this harvester might be in small surface craft, either manned or unmanned. Surface vessels typically have significantly higher space and weight margins than underwater vessels. On such a vessel, the size and weight of the harvester would not be as much of a concern, and the harvester would be exposed to surface wave action 100% of the time. Depending on the specific surface vessel, there may be room for a larger, heavier harvester or possibly many harvesters of the current size. If enough harvesters are installed, then supplementing or even recharging the main battery from the harvesters becomes an option. If a surface vessel application is pursued, the harvester parameters should be calibrated according to the sway acceleration of that specific vehicle instead of the bluefin-21 UUV.

THIS PAGE INTENTIONALLY LEFT BLANK

Chapter 5

Conclusion

In this thesis a novel oscillating energy harvester was designed to fit inside a Bluefin-21 UUV. Harvester performance was modeled using real world vessel acceleration data and optimized for four different potential energy profile configurations: free floating, linear monostable, nonlinear monostable, and bistable. It was confirmed that there is very little harvestable energy while the UUV is operating submerged below the surface wave action. Therefore, harvester was optimized for energy capture during periods when the UUV was drifting on the ocean surface. An active control strategy was desired, particularly for the bistable configuration, based on research from the MEMS community. Unfortunately, the two types of active control investigated, electromagnets and rotating permanent end magnets, were found to be too costly to implement and were abandoned. For each configuration the adjustable parameters of damping, spring stiffness, spring length, and end magnet force were optimized for energy capture.

The floating, linear, and bistable configurations achieved roughly the same results, with the linear harvester slightly edging the other two by $\approx 2.5\%$. The nonlinear harvester was found to be the least efficient configuration, collecting 12% less than the floating configuration. While the linear monostable model preformed the best, it

Configuration	Average Power W	Energy Harvested J/hr	b Ns/m	k_S N/cm	X_S cm	F_{Mmax} N
Floating	0.227	816	43	N/A	N/A	N/A
Linear	0.232	836	43	0.19	0	N/A
Non-Linear	0.200	720	49	N/A	N/A	37
Bistable	0.227	819	41	8.25	4.7	28.8

Table 5.1: Summary of Results

should be noted that these models where optimized for an excitation force extracted from a two minute interval of acceleration data. Ocean waves are notoriously broad-band and non-stationary in nature, and even a small change in sea state could result in detuning the linear harvester and a reduction in efficiency. For this reason, it is believed that the simpler free floating configuration is likely to meet or exceed the linear configuration over a range of sea state spectra.

The final result is an innovative and thoroughly studied alternative power source for UUV applications. While the calculated power collection rate was found to be insufficient as a means of supplementing or recharging the main batteries, the alternate function of supplying power to an emergency location beacon is a more reasonable application for the oscillating harvester. In this role, the harvester could essentially provide an indefinite "battery life" for the beacon, allowing continuous transmission as long as the UUV remained adrift, and thus aid in the recovery of a valuable asset. Recommended future work includes construction and testing of the harvester for comparison against the modeled results and continued research into control strategies.

Appendix A

A.1 Acronyms

AUV Autonomous Underwater Vehicle

AWG American Wire Gauge

emf Electromotive Force

FEMM Finite Element Methods Magnets

FOG INS Fiber Optic Gyro Inertial Navigation System

MEMS Micro-Electomechanical Systems

UUV Unmanned Underwater Vehicle

UV Underwater Vehicle

WEC Wave Energy Converter

A.2 Variables

A Area of the wire coil

A_j Constant in the fourier series fit function for the acceleration of the vessel

a Constant in the two term exponential function used to model the end magnet force

B Magnetic field strength

B_j Constant in the fourier series fit function for the acceleration of the vessel

b Total damping coefficient

C_j Combined amplitude of the fourier series constants A_j and B_j

c Constant in the two term exponential function used to model the end magnet force

ϵ Induced back emf in coils

F_B Bumper Force: force exerted on the slider by the rubber bumpers

F_C Control Force: force exerted on the slider by the control logic

F_emf Damping Force: force exerted on the slider by the back emf induced in the coils

F_E Excitation Force: force exerted on the slider by the vessel frame

F_M End Magnet Force: force exerted on the slider by the end magnets

F_{Mmax} Maximum end magnet force

F_S Spring Force: force exerted on the slider by springs

γ Coupling coefficient

$H_{\ddot{\xi}}$ Transfer function of the acceleration of the vessel

i Induced current in coils

j Indexing variable

k_B Stiffness coefficient of the rubber bumper

k_S Stiffness coefficient of the spring

m Mass of the slider, also know as the proof mass

P_L Power to the load, or the useful power harvested

P_{TH} Theoretical maximum power

Φ_B Magnetic flux

ω_j Frequency step in the fourier series fit function

ω_n Natural frequency

R_L Useful load resistance

R_C Parasitic resistance

S Spacing between the end magnet and the slider when up against the bumper

X_B Displacement where the slider will first contact the bumper

X_S Displacement where the slider will first contact the spring

x Displacement of the slider as measured from the center of the travel path

$\dot{x}$ Velocity of the slider with respect to the vessel frame

$\ddot{x}$ Acceleration of the slider with respect to the vessel frame

$\ddot{\xi}$ Acceleration of the vessel frame with respect to the Earth

Z Maximum displacement of the slider

THIS PAGE INTENTIONALLY LEFT BLANK

Bibliography

[1] D.P. Arnold. Review of microscale magnetic power generation. *IEEE Transactions on Magnetics*, 43(11), 2007.

[2] P. Carneiro, M.P. Soares Dos Santos, A. Rodrigues, J.A.F Ferreira, J.A.O. Simoes, A.T. Marques, and A.L. Kholkin. Electromagnetic energy harvesting using magnetic levitation architectures: A review. *Applied Energy*, 2020.

[3] C. Cepnik, O. Radler, S. Rosenbaum, T Strohla, and U. Wallrabe. Effective optimization of the electromagnetic energy harvesters through direct computation of the electromagnetic coupling. *Sensors and Actuators A: Physical*, 167, 2011.

[4] A.F. Falcao. Wave energy utilization. a review of technologies. *Renewable and Sustainable Energy Reviews*, 14(3):877–1134, 2010.

[5] Johannes Falnes. *Ocean Waves and Oscillating Systems*. Cambridge University Press, 2002.

[6] E. P. Furlani. Formulas for the force and torque of axial couplings. *IEEE Transactions on Magnetics*, 29(5), 1993.

[7] L. Gammaitoni, I. Neri, and H. Vocca. Nonlinear oscillators for vibration energy harvesting. *Applied Physics Letters*, 94(164102), 2009.

[8] E. Halvorsen, C.P. Le, P. Mitcheson, and E.M. Yeatman. Architecture-independent power bound for vibration energy harvesters. *PowerMEMS*, 2013.

[9] J. Heit and S. Roundy. A framework for determining the maximum theoretical power output for a given vibration energy. *Journal of Physics*, 557(012020), 2014.

[10] A.H. Hosseinloo and K. Turitsyn. Non-resonant energy harvesting via an adaptive bistable potential. *Smart Materials and Structures*, 25, 2016.

[11] Y. Jia. Review of nonlinear vibration energy harvesting: Duffing, bistablity, parametric, stochastic and others. *Journal of Inteligent Material Systems and Structures*, 31, 2020.

[12] JM Kim, MM Koo, JH Jeong, and et al. Design and analysis of tubular permanent magnet linear generator for small-scale wave energy converter. *AIP Advances*, 7, 2017.

[13] D. Mallick, A. Amann, and S. Roy. Surfing the high energy output branch of nonlinear energy harvesters. *Physical Review Letters*, 117(197701), 2016.

[14] B.P. Mann and N.D. Sims. Energy harvesting from the nonlinear oscillations of magnetic levitation. *Journal of Sound and Vibration*, 319:515–530, 2009.

[15] Arthur Pecher and Jens Peter Kofoed. *Handbook of Ocean Wave Energy*, volume 7 of *Ocean Engineering and Oceanography*. Springer International Publishing, Switzerland, 2017.

[16] M. Penalba and J.V. Ringwood. Review of wave-to-wire models for wave energy converters. *Energies*, 2016.

[17] S.M. Shahruz. Design of mechanical band-pass filters for energy scavenging. *Journal of Sound and Vibration*, 292:987–998, 2006.

[18] N.G. Stephen. On energy harvesting from ambient vibration. *Journal of Sound and Vibration*, 293:409–425, 2007.

[19] D. Su, R. Zheng, K. Nakano, and P.C. Matthew. On square-wave-driven stochastic resonance for energy harvesting in a bi-stable system. *AIP Advances*, 4, 2014.

[20] Matt Tearle. Simple real fourier series approximation. https://www.mathworks.com/matlabcentral/fileexchange/31013-simple-real-fourier-series-approximation. Accessed: 2023-03-05.

[21] Electronics Tutorials. Knuth: Computers and typesetting. http://www.electronics-tutorials.ws/power/three-phase-rectification.html. Accesses: 2023-02-18.